IOP PUBLISHING METROLOGIA
Metrologia **46** (2009) 512–524 doi:10.1088/0026-1394/46/5/016

Reduced non-linearities and improved temperature measurements for the NIST Johnson noise thermometer*

Jifeng Qu[1], S P Benz[1], H Rogalla[2] and D R White[3]

[1] National Institute of Standards and Technology, 325 Broadway, Boulder, CO 80305, USA
[2] Department of Applied Physics, University of Twente, PO Box 217, 7500 AE Enschede, The Netherlands
[3] Measurement Standards Laboratory, PO Box 31310, Lower Hutt, New Zealand

Received 15 May 2009, in final form 3 July 2009
Published 31 July 2009
Online at stacks.iop.org/Met/46/512

Abstract
The variance of temperature measurements made with the NIST Johnson noise thermometer has been reduced by the use of improved cross-correlation electronics and a unique method for measuring and reducing non-linearities. The spectral response of the voltage noise and the reproducibility of the measured temperature were improved by the use of a lower-noise preamplifier with better common-mode rejection and by removal of a systematic aliasing error through additional filtering. Even with these improvements, however, measurements with precision multi-tone comb and two-tone waveforms, which were synthesized with the quantum voltage noise source, showed that distortion generated by non-linearities in the electronics still limited the measurement standard deviation to (3–5) μK/K greater than that expected for uncorrelated white noise. The new electronics and the measurement techniques used to characterize the non-linearities are described. Synthesized waveforms that have higher tone density are shown to reduce the distortion generated by the remaining non-linearities so that the variance of the measurement is no longer limited and continues to decrease with measurement time as expected.

(Some figures in this article are in colour only in the electronic version)

1. Introduction

In Johnson noise thermometry (JNT), an unknown temperature is determined by measuring the thermally induced Johnson noise voltage generated across a sensing resistor. The temperature is related to the voltage noise V_R through the Nyquist equation, $\langle V_R^2 \rangle = 4kTR\Delta f$, where k is Boltzmann's constant, T is the temperature, R is the resistance of the resistor and Δf is the measurement bandwidth [1–3]. The main challenge of JNT is that it requires accurate, low-noise electronics, typically using cross-correlation techniques, to measure the small voltages, such as the 1.2 nV $\mathrm{Hz}^{-1/2}$ voltage noise of a 100 Ω resistor at the triple point of water, $T_{tpw} \equiv 273.16$ K. The NIST JNT system uses quantum-accurate pseudo-noise voltage waveforms synthesized by a superconducting quantum voltage noise source (QVNS) as a reference noise source. These multi-tone comb waveforms provide an accurate reference over the measurement bandwidth and enable the cross-correlation electronics to be calibrated [4–8]. The harmonic frequencies and amplitudes of the sinusoids that compose the synthesized time-dependent voltage waveforms are chosen so the calibration noise power and spectral density closely match the noise power of the sensing resistor. The output impedance of the QVNS is chosen to match that of both the sensing resistor and the output transmission line [4–7]. These features reduce the measurement uncertainty, increase the measurement bandwidth and decrease the measurement time.

The JNT system can be used to make an absolute measurement of an unknown temperature or to infer a value of Boltzmann's constant [9]. In either application, the combined measurement uncertainty is dominated by the variance in the mean of the ratio of the measured power spectral densities of the sensing resistor's thermal noise and the voltage

* US government work, not protected by US copyright.

waveform synthesized by the QVNS. Recent improvements to the system include lower-noise preamplifiers with increased common-mode rejection (CMR), higher cut-off frequency filters for broader bandwidth, grounded QVNS circuits, QVNS waveforms with higher tone density and improved matching between the QVNS and sensing resistor circuits for both noise-power and transmission-line transfer functions [9]. All these improvements allowed the NIST JNT system to make the first absolute temperature measurement of the water triple point in terms of h/e with a 19 μK/K statistical uncertainty in less than 36 h [9–11]. However, the standard deviation in the mean power ratio must be reduced to five parts in 10^6 before JNT measurements can practically contribute to a re-determination of Boltzmann's constant [12].

This paper describes further improvements to the measurement electronics as well as a new technique for detecting non-linearities that exploits the inherent low-distortion and arbitrary waveform-synthesis features of the QVNS. Both improvements contribute to reducing the measured variance through a better calibration and control of the frequency response of the measurement. The measurement electronics were improved in two different ways: first, by the use of a preamplifier design that provides better CMR and a slightly lower noise floor, and second, by the use of additional passive filter and buffer amplifier stages that remove a systematic aliasing error that affected the measurement reproducibility. The new preamplifier design and performance features are described in detail in the appendix. The non-linearity measurement technique, which is described in section 3, was developed to characterize and reduce the distortion produced by non-linearities throughout the JNT system.

Distortion produced by non-linearities has two measurable effects: it limits the measured variance of the QVNS-synthesized voltage noise, which otherwise is defined to produce a constant power spectral density, and it can produce a systematic error in the measured temperature. Non-linearities in various parts of the cross-correlation electronics have been a continuing challenge throughout the development of the NIST JNT system [9] and, until this paper, remained one of the most challenging problems limiting the performance of the JNT. Finding and eliminating sources of non-linearity is a challenging task, because the distortion is extremely small and is usually hidden below noise floors of both the amplifiers and the cross-correlated QVNS signal. Some of the previously identified sources of distortion in the measurement circuit and electronics, which were found through careful analysis of auto- and cross-correlation measurements, were damaged components, wiring connections, oxidized solder, kinked wires and even some multifilament wires [7, 9]. The preamplifier is probably the most important circuit component in the JNT system [13], and the effects of amplifier non-linearity on the performance of JNT systems have been thoroughly investigated for the white random noise of sensing resistors [14]. The response of the amplifier and cross-correlation electronics to the pseudo-noise waveforms synthesized by the QVNS were evaluated more recently [10, 11, 15]. The investigation of non-linearities presented in this paper complements these results.

Synthesized waveforms such as those generated by the QVNS are a powerful tool for evaluating non-linearities in the JNT electronics, because they can be synthesized with a wide range of amplitudes and harmonic content, with no change in the circuits. For example, Toonen and Benz demonstrated that quantum-accurate synthesized two-tone waveforms can be used to characterize the non-linearity of signal processing components [15]. Their measurements of the preamplifier stage of the NIST JNT system showed a spurious-free dynamic range of about 67 dB with a maximum input signal of about −42 dBmV. For smaller input signals, the distortion remained hidden below the noise floor of the amplifier.

This paper describes how the frequency response and non-linearities of the JNT electronics were improved and optimized by performing a variety of measurements of two-tone and multi-tone QVNS-synthesized waveforms with different amplitudes and harmonics. As expected, it was found that the second-order inter-modulation (IM) and harmonic distortion are more significant than the third-order IM distortion. A systematic error caused by aliasing of the stop band of the low-pass filters (LPF) is described in section 3. Finally, in section 4 it is shown that the remaining dominant harmonic distortion, at least for multi-tone odd-harmonic-only waveforms, is caused by non-linearities in the analogue-to-digital converters (ADCs), and that the distortion can be minimized by the use of synthesized waveforms with higher tone density.

2. QVNS and cross-correlation electronics

Waveforms for the QVNS are produced with digital codes generated with delta–sigma analogue-to-digital conversion algorithms. The QVNS synthesizes precision waveforms that are intrinsically accurate because the voltage pulses produced by the Josephson junctions are always perfectly quantized and have a time-integrated area precisely equal to the inverse Josephson constant $K_J^{-1} \equiv h/2e$, the ratio of Planck's constant to twice the electron charge [4, 16, 17]. The QVNS circuit consists of a symmetric pair of grounded, lumped arrays having a small total number of junctions (typically $N_J = 8$ to 256). The chip used in the current JNT experiments contains two arrays each having only four superconductor/normal-conductor/superconductor (SNS) Josephson junctions. Each array is separately biased by a unipolar pulse drive that is clocked at the 10 GHz sampling frequency f_s. The synthesized waveform has a minimum frequency called the pattern-repetition frequency, $f_0 = f_s/M$, that is determined by the clock frequency and the bit length M of the digital waveform. Pseudo-noise waveforms, typically even-only or odd-only frequency combs, are constructed by summing equal-amplitude, random-phase harmonics of f_0. The amplitudes of these tones are chosen to closely match the power spectral density of the sensing resistor. Two-tone waveforms for non-linearity characterization are constructed from a pair of fundamental frequencies f_1 and f_2, which are also harmonics of f_0. The frequency values of f_1 that are used in this paper are 30 kHz, 100 kHz and 300 kHz, while f_2 was defined to be always 800 Hz greater than f_1. For each frequency, different codes were generated so as to produce different single-tone

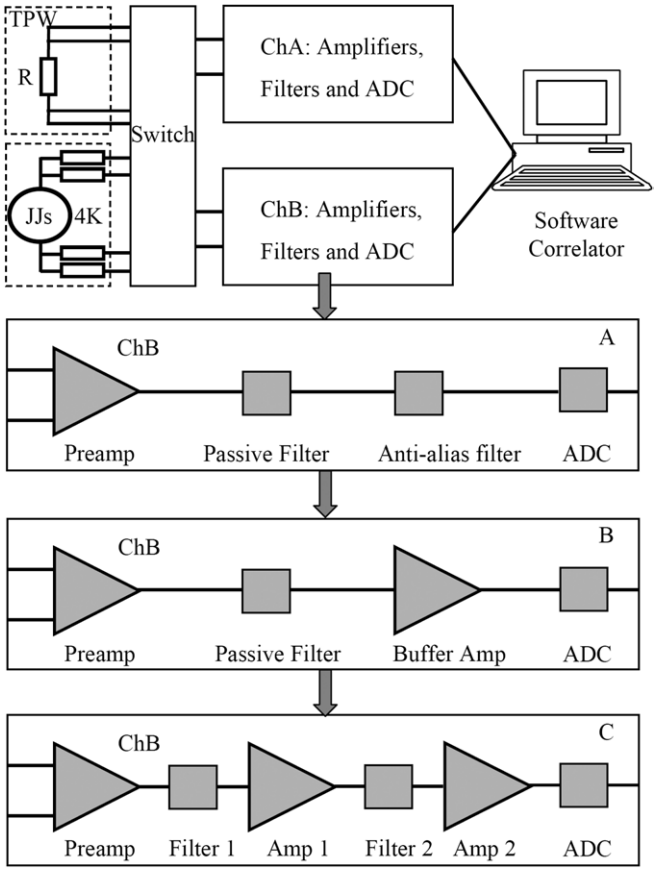

Figure 1. Schematic drawing of the JNT cross-correlation electronics with different versions (A)–(C) of the amplifier–filter chain.

amplitudes ranging from 1 μV to $4\sqrt{2}$ μV. The phases of the two sine wave tones were chosen to have zero relative phase at the beginning of each code sequence. Different waveforms, either multi-tone combs or two-tones, were used to reveal the frequency- and amplitude-dependent harmonic distortion effects of non-linearities, and the results are described in section 3.

Figure 1 shows a schematic drawing of the JNT cross-correlation electronics. It consists of two nominally identical channels. Depending on the position of the switching network, the resistor and QVNS-synthesized voltage signals in each channel are alternately amplified, filtered and measured with an ADC. Three different circuit configurations (A)–(C) of the amplification circuits were used in the last two years, and are illustrated in figure 1. The preamplifier, which is described in detail in the appendix, has a CMR of about 100 dB at 100 kHz and a 0.85 nV $\mathrm{Hz}^{-1/2}$ noise floor. In measurements prior to 2006, the measurement bandwidth was defined by a 4-pole digital filter that had a 150 kHz cut-off frequency and was used in conjunction with a 2 MHz active anti-alias filter, which was used to prevent aliased signals from adding to the noise power in the low-frequency measurement range. In 2007, the measurement bandwidth was increased to 650 kHz by replacing the digital filter with the circuit shown in configuration A, which has an 11-pole LPF. In circuit B, the anti-alias filter was replaced with a buffer amplifier with a 5.5× gain (at 50 Ω) to eliminate large even-order distortion that was occurring in the active anti-alias filter. The buffer amplifier in configuration B was added in order to maintain the same total gain for the amplifier chain in each channel, which is required to drive the ADC at the optimum dynamic range. Circuit C, whose improved performance is described in the next section, uses two low-pass filters each having 11 poles, with different respective cut-frequencies of 650 kHz and 800 kHz. The second filter compensates for the limited stop band of the first filter and ensures that the aliased tones in the 650 kHz passband are more than 120 dB lower than the synthesized fundamental tones. Correspondingly, two buffer amplifiers (1 and 2) with 1× and 5.5× gains (at 50 Ω) are used to drive the second filter and the ADC. In each circuit the same 14-bit ADC samples the signal for 1 s periods with a 2.08 MSa s^{-1} sampling frequency. Fast Fourier transforms (FFTs) of the signals are then computed, yielding 1 Hz frequency-resolved FFT bins and a 1.04 MHz Nyquist frequency f_N. The measured signals from both channels are then cross-correlated in software to reduce the uncorrelated noise from each channel. The ADC has a 2.2 V peak-to-peak differential input voltage range and differential and integral non-linearity specifications of ±0.25 least significant bit (LSB) and ±0.5 LSB, respectively.

The temperature is determined from the cross-correlated electrical and thermal noise powers measured over discrete bandwidths centred at each QVNS tone. The bandwidth around each tone depends on the tone spacing of the synthesized waveform, e.g. $2f_0$ for odd- or even-tone combs. The ratio of the mean square voltage noise at each tone frequency, $\langle V_\mathrm{R}^2\rangle/\langle V_\mathrm{Q}^2\rangle$, can be used to separately evaluate the absolute temperature:

$$T = \left(\frac{\langle V_\mathrm{R}^2\rangle}{\langle V_\mathrm{Q}^2\rangle}\right)\frac{D^2 N_\mathrm{J}^2 f_\mathrm{s} M}{4kX_\mathrm{R}R_\mathrm{K}K_\mathrm{J}^2}, \qquad (1)$$

where resistance is expressed as the ratio X_R in units of the von Klitzing resistance $R_\mathrm{K} \equiv h/e^2$ [18], and D is a QVNS waveform-synthesis parameter, chosen exactly, that is used to closely match the power spectral densities. Thus, the temperature can be determined from known constants and measurements of the sensor resistance and synthesized noise voltages.

In practice, the frequency-dependent noise-power ratio in (1) is fitted with a two-parameter model ($a_0 + a_2 f^2$, a_2 is typically $\sim 10^{-9}\,\mathrm{kHz}^{-2}$), to remove the small remaining differences in the frequency responses of the transmission lines connecting the resistor and QVNS circuits to the preamplifiers, because the transfer functions are matched only to about a part in 10^3 at 600 kHz. The parameter a_0, which is the average power ratio corrected for the frequency dependence, is then used to calculate the temperature. The statistical contribution to the uncertainty in the temperature measurement, arising from the random properties of the thermal noise signal and the noise in the preamplifiers, is also determined from the fit as the standard deviation in a_0. As the measurement time is increased and more cross spectra are averaged, the standard deviation is expected to fall as the inverse of the square root of the total integration time. The measured standard deviation, which

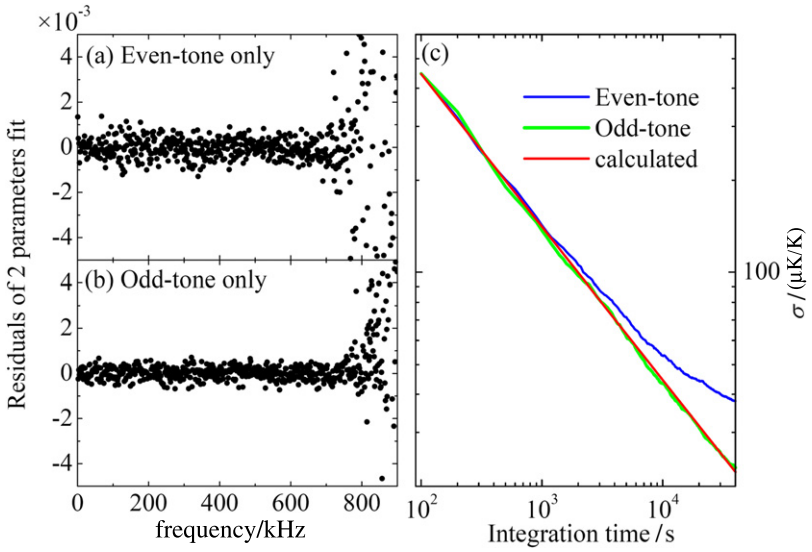

Figure 2. Residuals of two-parameter fits of the resistor-QVNS power ratio for circuit configuration C and waveforms with $f_0 = 400\,\text{Hz}$ and (*a*) even-only and (*b*) odd-only harmonic tones. (*c*) The standard deviation for the two measurements as a function of time for the data in the 4 kHz to 600 kHz frequency range. The standard deviation for the temperature measurement with even tones saturates with increasing integration time. The theoretically expected statistical standard deviation calculated with equation (38) in [11] is also shown for comparison.

includes additional distortion-induced scatter in the measured QVNS spectra (see section 3), was monitored and compared with a theoretical value calculated with equation (38) of [11].

3. Frequency response and distortion

Prior to the experiments described in this paper, the NIST JNT system used QVNS pseudo-noise waveforms that contained only odd-harmonic tones [4–9]. Waveforms with all or even-only harmonic tones were not used, because measurements of the resistor-QVNS power ratio using these waveforms were scattered, with greater variance than expected from theory, across the entire measurement bandwidth. Residuals of two-parameter fits of the thermal-QVNS spectral ratios for odd-tone and even-tone QVNS waveforms with $f_0 = 400\,\text{Hz}$ are, respectively, shown in figures 2(*a*) and (*b*). Figure 2(*c*) shows the measurement standard deviation, calculated over the range 4 kHz to 600 kHz, versus integration time for these two measurements performed with electronics configuration A. The expected standard deviation is also shown.

In the measurements that use the even-tone pseudo-noise waveforms, further integration of the data does not significantly reduce the standard deviation, and the measurement variance is limited, indicating that the measurement variance is dominated by *random amplitude correlated signals* due to distortion products. This effect becomes apparent in the measured QVNS spectrum for three reasons. Firstly, because the distortion products are the same for each repetition of the QVNS waveform, they accumulate in the averaged spectra. Secondly, the large relative amplitude of the QVNS tones means the distortion products are larger and located at relatively few spectral locations, making them visible above the noise floor. Finally, for even-tone QVNS spectra, the most prominent second-order distortion products fall on top of QVNS tones, which amplifies their effects in the power measurements (see below). If the odd-harmonic QVNS waveforms are used, the same effect occurs but the saturation emerges at lower standard deviations and after a longer integration time. The same distortion occurs in the thermal noise spectra, but the distortion products are dispersed over all frequencies, and are not correlated over time so that their measured amplitudes fall, along with uncorrelated noise, in proportion to the square root of the integration time.

The distortion effects observed in the QVNS spectra suggest that the non-linearities of the JNT electronics produce larger second-order than third-order distortion. In order to improve the measurement standard deviation and perform practical temperature measurements, odd-harmonic QVNS waveforms were required when the electronics produced large harmonic distortion while the QVNS signals were measured.

3.1. *Effects of distortion on QVNS spectra*

Non-linearities in electronic systems cause the mixing of signals at different frequencies and the generation of distortion products at frequencies different from the source signals. For example, second-order distortion of signals at frequencies f_1 and f_2 generates distortion products at frequencies $f_1 \pm f_2$, $2f_1$, $2f_2$ and 0 Hz. In general, Nth-order distortion of a signal with components at f_1, f_2, f_3, ..., f_N generates distortion products at the frequencies $k_1 f_1 + k_2 f_2 + \ldots + k_N f_N$, where the k_i are integers such that $|k_1| + |k_2| + \ldots + |k_N| = N$. For the moment we consider only second- and third-order distortion, as they are representative of the effects of even- and odd-order distortion, respectively, on the different QVNS waveforms. There are several permutations to consider.

Consider first the effects of second-order distortion on a QVNS spectrum comprising only even tones at the frequencies $2f_0$, $4f_0$, $6f_0$, ... The distortion, such as caused by a component generating an error exactly proportional to the voltage squared, generates unwanted products at

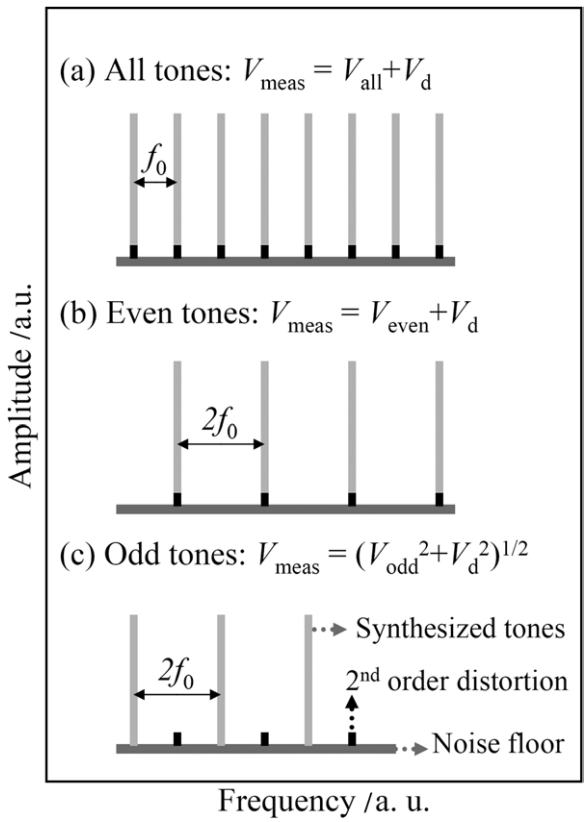

Figure 3. Schematic FFT diagram showing the relative frequency position of synthesized tones (grey) and second-order distortion harmonics (black) for different multi-tone comb waveforms. The third-order distortion is much lower than the second-order distortion and is not displayed. For *all*-tone (*a*) and *even*-tone (*b*) QVNS waveforms, the second-order distortion contributes directly to the measured voltage at each frequency. For the *odd*-tone waveforms (*c*), the distortion contributes only as the root-sum-square to the measured voltage.

frequencies that are the sums, differences and multiples of these frequencies, all of which are also even multiples of f_0. That is, the unwanted distortion products are positioned on top of the QVNS tones. In fact, multiple distortion products are positioned on top of every QVNS tone. For example, on top of the $2f_0$ tone there will be a distortion product arising from every adjacent pair of tones. Since every tone has a random phase, all of the distortion products will add randomly to give rise to a cumulative distortion product of random amplitude and random phase with respect to the QVNS tone at that location. The effect of distortion on waveforms with all (both odd and even harmonic) tones will behave similarly to that for the even-tone waveforms.

Now consider the effects of second-order distortion on a QVNS spectrum comprising odd tones at the frequencies $f_0, 3f_0, 5f_0, \ldots$. Again, the distortion will generate products that are the various sums, differences and multiples of these frequencies, all of which are again even multiples of f_0. That is, the distortion products are positioned at frequencies between the QVNS tones. The effects of the second-order distortion are summarized in figure 3. Third-order distortion, unfortunately, makes no distinction between the different QVNS spectra: the sums and differences of three odd or even frequencies remain odd or even, respectively. Note that, so long as the same QVNS signal is used for all measurements, and the distortion in each channel of the correlator is constant, the features in the spectrum due to the distortion products will also be constant.

Suppose that the cumulative distortion products are modelled as a sinusoid with a complex voltage $V_{QVNS}(x + iy)$ that is random with respect to the frequency of the QVNS tone, but fixed in time. V_{QVNS} is the voltage of each QVNS tone and the variables x and y are fractions very much smaller than 1. To simplify the mathematics, we also assume that the distortion produced in each channel of the correlator is identical and constant. When the distortion product is positioned away from the QVNS tone, such as the second-order distortion for odd-tone waveforms, the calculated power due to the QVNS for the block of FFT bins in the cross-correlation spectrum located near a tone is

$$V_{QVNS}^2 + V_{QVNS}^2 |x + iy|^2 = V_{QVNS}^2 (1 + x^2 + y^2). \quad (2)$$

Thus, the distortion products introduce a random component to the calculations of power for each QVNS tone. If the distortion product falls on top of the QVNS tone, such as the second-order distortion for even-tone waveforms, then the calculated power is

$$V_{QVNS}^2 |1 + x + iy|^2 = V_{QVNS}^2 (1 + 2x + x^2 + y^2). \quad (3)$$

The distortion product therefore induces a much greater fractional variation in the measured QVNS power when it falls on top of a QVNS tone. Note too that the variable x has zero mean when averaged over all QVNS tones. It will therefore not cause a significant bias in the temperature measurement. Because they have non-zero mean, the remaining terms of $x^2 + y^2$ do cause a small bias. Calculations by White and Mason for typical resistor–resistor [14] and also for QVNS-based [10] JNT measurements showed that only odd-order non-linearities affect the temperature measurement, while even-order non-linearities have a negligible effect. Commutation of the preamplifier inputs was also shown to completely eliminate the effect of even-order non-linearities [10, 14]. The effect of any remaining non-linearity is reduced by ensuring that the resistor-QVNS power ratio, $\langle V_R^2 \rangle / \langle V_Q^2 \rangle$, is very close to unity, ensuring that the distortion affects the QVNS spectrum and the resistor noise spectrum in the same way. Thus, for example, matching the noise power ratio to 0.1% and ensuring that the distortion products are all below 0.1% would ensure that the overall effect of the distortion is kept to 0.0001%.

3.2. Reducing non-linearities and aliasing effects

The QVNS system enables a number of tests for distortion, including searching for outlying spectral features between tones of an odd-tone QVNS spectrum, and the increased standard deviation caused by the distortion, especially for second-order distortion acting on the even-tone QVNS spectrum. For example, while measurements were performed with odd-tone waveforms, large even-order distortion was observed above the noise floor in the spectral measurements

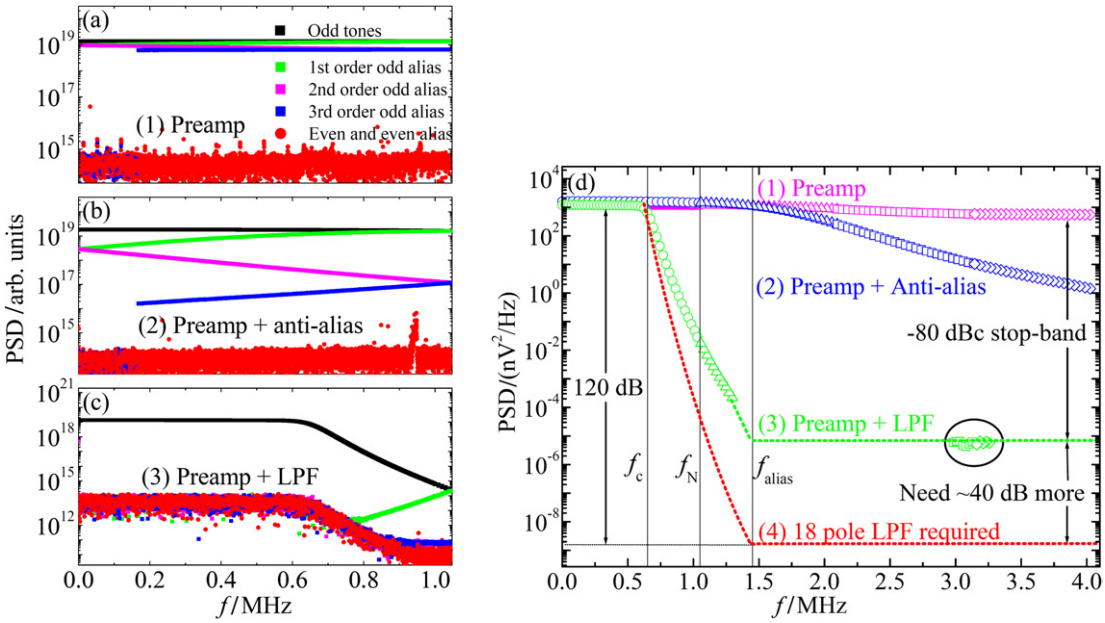

Figure 4. Measured power-density spectra for different measurement component combinations. (*a*) Preamp board only, (*b*) preamp + anti-alias boards and (*c*) preamp + 650 kHz LPF (no anti-alias filter). (*d*) Transfer functions reconstructed from multiple-alias harmonics extracted from (*a*)–(*c*). Triangles, squares and diamonds represent higher-order aliased tones. The fourth plot of dotted lines indicates the transfer function needed to ensure that no aliased signals affect measurements of the noise power below 650 kHz.

of the QVNS signals only after measuring for long integration times. By replacing various circuit components and circuits, many of the largest sources of harmonic distortion were removed, including the active anti-alias filters (configuration A) that introduced large even-order distortion that was possibly caused by non-linearities from damaged but still functioning components. After removing these active amplification circuits, the even harmonic distortion was dramatically reduced (for circuit configuration B).

While amplifier–filter configuration B was used [9], an additional problem was found: the 11-pole LPF was found to have a stop-band attenuation of only −80 dBc (80 dB lower than the fundamental tones). The transfer functions for (1) the preamplifier, (2) the preamplifier plus the anti-alias board (circuit A, but without the passive filter) and (3) the preamplifier plus the 11-pole filter, which has a 650 kHz cut-off frequency, were also measured (circuit B). The left panel ((*a*)–(*c*)) of figure 4 shows the measured frequency responses of the same pseudo-noise waveform, which contained only odd-harmonic tones, for these three different amplifier–filter configurations. Multiple aliases can be clearly seen in figures 4(*a*) and (*b*). In figure 4(*c*), because of the faster roll-off of the passive filters, the multiple aliases are just resolvable above the noise floor in the 0.8 MHz to 1.0 MHz baseband frequency range. To elucidate the frequency response, the circuits' transfer functions were reconstructed from the baseband frequency bins that contained the measured multiple aliases of the QVNS tones, which were synthesized up to 4 MHz. Figure 4(*d*) shows the reconstructed transfer functions up to 4 MHz for each of these amplifier–filter configurations. The faster roll-off of the passive filter is noticeable, as are the (circled) −80 dBc aliased signals of the stop band near 3 MHz. A dotted line shows the expected transfer function and stop-band level that was hidden by amplifier noise.

These results expose an interesting experimental challenge: the stop-band signals must be at least −120 dBc (40 dB lower), so that the aliased signals from the stop band, which could extend to several megahertz or more, contribute less than a part in 10^6 to measurements of the desired voltage noise signals. To achieve such a stop band, a higher-order filter (at least 18 poles) is needed, so that signals at and above the alias frequency $f_{\text{alias}} = 1.43$ MHz, when aliased below the filters' cut-off frequency f_{C}, do not contribute to the measured power. Unfortunately, passive 18-pole filters do not have sufficient stop-band attenuation. Thus, in order to ensure that the aliased stop-band signals do not add into the low-frequency noise spectrum, a second passive filter and another buffer amplifier were added, as shown in circuit configuration C. This second filter is also an 11-pole LPF, but with a higher, 800 kHz cut-off frequency compared with the first filter.

Figure 5 presents the residuals for resistor-QVNS measurements for QVNS waveforms with odd-only and even-only harmonic tones with the new circuit configuration C. This circuit contains no aliased stop-band error and has lower harmonic distortion than that of circuit configuration A that contained the active anti-alias filter. The random scatter of the residuals of the two-parameter fits of the resistor-QVNS power ratio for the even-tone waveform is now greatly reduced, and no distinct difference can be observed between waveforms with odd-only and even-only harmonic tones after integration for 40 000 s, as shown in figures 5(*a*) and (*b*). Moreover, in figure 5(*c*) one can see that the measurement standard deviation no longer saturates with increasing integration time for either of the waveforms, which is a dramatic improvement compared with the results shown in figure 2(*c*) with circuit configuration A. However, the measurement standard deviation for the even-tone waveform

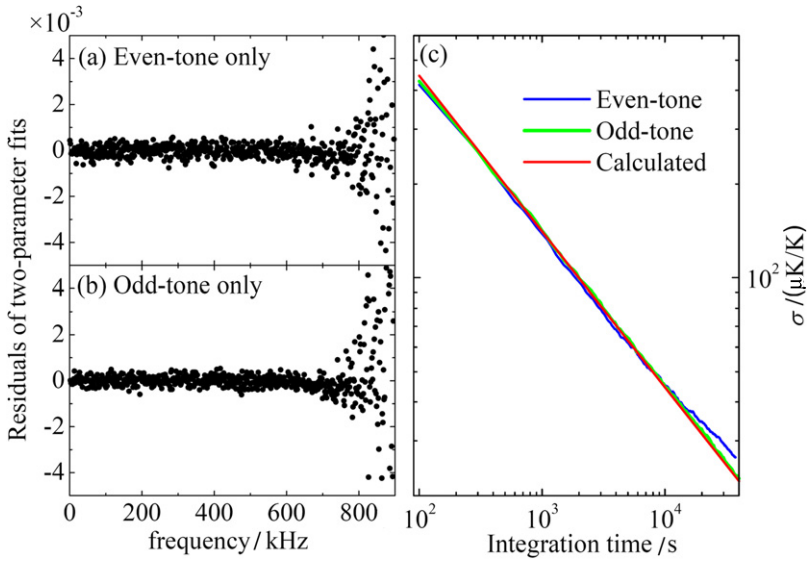

Figure 5. Residuals of two-parameter fits of the resistor-QVNS power ratio after integrating for 40 000 s for waveforms with $f_0 = 400$ Hz and only (*a*) even and (*b*) odd-harmonic tones for the new cross-correlation electronics (configuration C). (*c*) The expected statistical standard deviation for white noise and the standard deviation for measurements of QVNS waveforms with only even and odd tones.

at the longest integration times is still slightly higher than that for the odd-only harmonic-tone waveform, indicating that the electronics non-linearities remain dominated by even-order distortion.

3.3. Characterizing non-linearities with two-tone waveforms

In fact, only a few small-amplitude distortion tones are observable at high frequencies for circuit C in the measured auto- and cross-correlation spectra of QVNS-synthesized pseudo-noise multi-tone combs. Most of the remaining intrinsic non-linearities of the electronics are so small that the even harmonic distortion for odd-only comb waveforms is buried deeply below the noise floor, even for cross-correlation integration times of several days, which makes it difficult to further improve the non-linearity performance of the JNT electronics. In order to measure the remaining distortion, larger amplitude two-tone waveforms were used so that the amplitudes of some distortion harmonics were greater than the amplifier noise floor for auto-correlation measurements of each channel. Cross-correlation measurements with integration time of around 15 h were also performed to observe the lower-amplitude distortion harmonics. Figure 6 shows the auto- and cross-correlation measurements of a synthesized waveform with two tones (300.0 kHz and 300.8 kHz) with 4 μV rms amplitudes and zero relative phase. Note that the auto-correlation noise floor is below 1 nV $\mathrm{Hz}^{-1/2}$. This low noise floor, provided by the new preamplifier and the 1 Hz resolution of the JNT electronics, allowed us to observe the distortion with a small 4 μV input voltage. However, this distortion was not observed with the previous ACJVS measurements that were sampled with a different instrument [15].

The different distortion products in figure 6 are represented with different symbols. The fact that the distortion harmonics are at or below the auto-correlation noise floor in this plot emphasizes the difficulties in measuring such

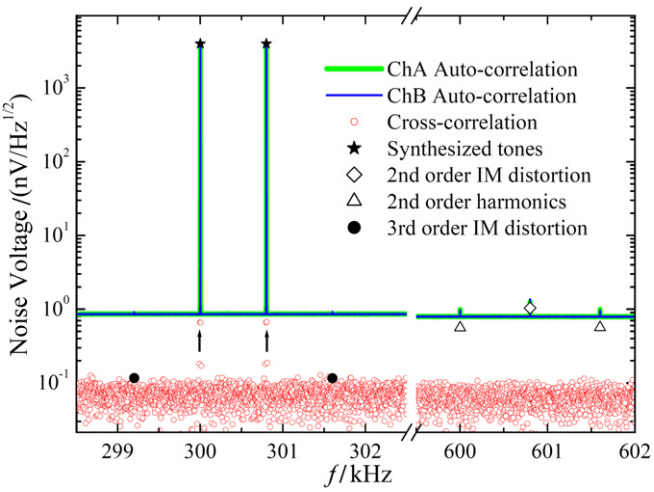

Figure 6. Auto- and cross-correlation power spectral density of a QVNS-synthesized two-tone waveform. Second- and third-order IM distortion and second-order harmonics are indicated with different symbols. The arrows pointing to pairs of 1 Hz bins indicate the presence of phase noise from either the QVNS source or ADC measurement clocks.

small non-linearities. For the third-order IM distortion, the tones are practically invisible in the auto-correlated data (just above the noise floor). Cross-correlating the signal reveals the presence of distortion in both channels. Unfortunately, the cross-correlated data provide only a qualitative result that indicates the presence of distortion, because the distortion is not necessarily correlated for the different channels. The third-order IM distortion is about three times lower than what was observed in the 2007 circuit of configuration A [9]. It is very important to note that the second-order distortion, both from the harmonics and the IM distortion, is much larger than the third-order distortion. This same result was found in measurements that were made with the previous version of electronics [9] and in [15].

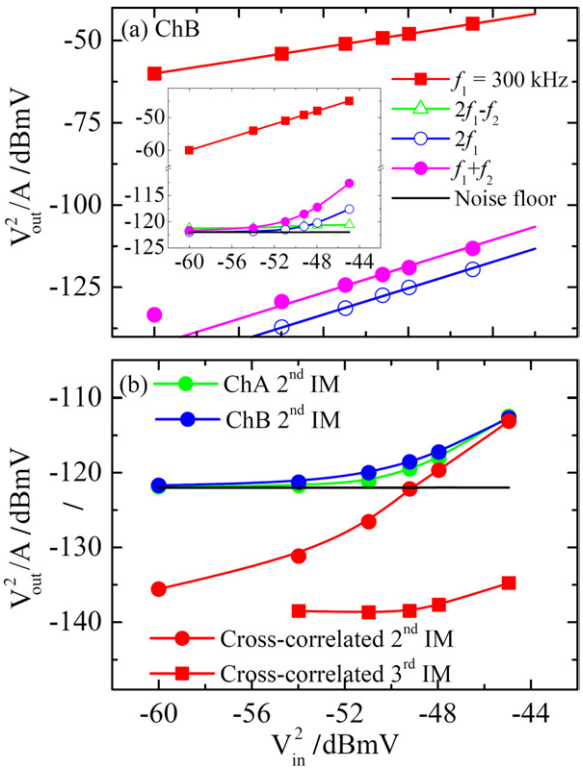

Figure 7. Fundamental and harmonic distortion responses as a function of input amplitude for two-tone synthesized waveforms with $f_1 = 300$ kHz and with $f_2 = 300.8$ kHz. (*a*) The auto-correlated signals for channel B with the noise floor subtracted (inset shows the total measured voltage amplitudes and a line indicates the noise floor). (*b*) The output fundamental tone and associated second- and third-order IM distortion from both the auto- and cross-correlation measurements.

Further investigation of the distortion characteristics is helpful for identifying the sources of the remaining non-linearities. Auto- and cross-correlation measurements were carried out on waveforms with different amplitudes in the range of (1 to $4\sqrt{2}$) μV. For waveforms with tone amplitudes below 1 μV, the amplitudes of the distortion tones are too small to be clearly resolved. Furthermore, waveforms with amplitudes larger than $4\sqrt{2}$ μV cannot be used because the amplified output signals exceed the full-scale range of the ADC.

The inset of figure 7(*a*) shows the auto-correlated amplified output signal and distortion responses to input power that were measured with channel B of the JNT electronics with a two-tone waveform with $f_1 = 300$ kHz. The distortion signals are close to the noise floor, and are difficult to evaluate, especially the third-order IM distortion. The non-inset data of figure 7(*a*) show the output fundamental and distortion amplitudes with the noise floor contribution subtracted. Since the noise voltage has random phase, the time average of the voltage product between the fundamental tone and the noise floor is zero, so that $\langle V_d^2 \rangle = \langle V_{meas}^2 \rangle - \langle V_{noise}^2 \rangle$. The extracted harmonic distortion voltages V_d follow the expected linear behaviour with appropriate slopes of two for both second-order IM and harmonic distortion. It was not possible to properly extract and fit the third-order IM distortion, because the signals were too small compared with the noise. The extrapolated intercept points are useful to characterize the amplification circuits: the second-order IM intercept point IP2 is 95 dBmV for channel B and 96 dBmV for channel A.

In order to ensure that the measured standard deviation resembles the expected statistical standard deviation, it is necessary to reduce the amplitude of the distortion products to an acceptable value. The distortion-induced scatter will contribute less than a part in 10^6 to the standard deviation provided that the real part of the vector sum of the distortion products at each tone frequency is approximately 120 dB below the magnitude of that tone. For a JNT multi-tone comb with 800 Hz spacing between adjacent tones, the amplitude of the tones that matches the thermal noise across a 100 Ω resistor at the T_{tpw} is about 35 nV (−89 dBmV). By extrapolating the fit of the second-order IM distortion, the distortion for 35 nV two-tone waveforms is estimated to be around 110 dB below that of the synthesized tones. For multi-tone comb waveforms of the same amplitude, the distortion may be higher, because different pairs of tones produce distortion at the same frequency, and the accumulated distortion may be much larger than this value, depending on the relative phases of the contributing distortion components.

Figure 7(*b*) shows the amplitude responses of the measured auto-correlation signals in both channels and the cross-correlation signals of the second- and third-order IM distortion for the two-tone waveform with $f_1 = 300$ kHz. To further understand the behaviour of the non-linearity, similar measurements were performed for waveforms with $f_1 = 30$ kHz and 100 kHz. Both the second- and third-order non-linearities were found to increase with increasing frequency. Over the entire frequency range of measurements, the cross-correlated second-order distortion is much higher than the third-order distortion. The results confirm that the non-linearities in each channel have different magnitude and phase response. For example, the second-order IM distortion is lower in channel B than in A for $f_1 = 30$ kHz and 100 kHz (it can hardly be seen in channel B for 30 kHz), while it becomes higher in channel B than in A for $f_1 = 300$ kHz. This indicates that the distortion comes from different circuits or circuit components in each channel. If the sources of non-linearity can be found, it may be possible to further reduce the distortion.

In yet another attempt to determine the source of remaining non-linearities in the hope of reducing or removing it, further measurements were made with the JNT cross-correlation electronics of odd-only multi-tone waveforms with $f_0 = 400$ Hz and amplitude of each tone ∼35 nV. The spectra of this waveform displayed only a few remaining small even-order distortion tones above 800 kHz. The source of the distortion within the JNT electronics could not be located, so the FFT of the resulting signal at different points in each channel's amplifier chain was measured with a National Instruments (NI) 5922A digitizer[4] and the same odd-only multi-tone comb. Interestingly, the distortion tones found

[4] Commercial instruments are identified in this paper only in order to adequately specify the experimental procedure. Such identification implies neither recommendation nor endorsement by the National Institute of Standards and Technology, nor that the equipment identified is necessarily the best available for the purpose.

with the JNT ADC were not observed in the spectra measured with NI digitizer in any of the amplification stages, including an input amplifier (not shown in figure 1) that is part of the JNT ADC. These results suggest that the observed distortion tones above 800 kHz were produced by the ADC. In order to further investigate the ADC non-linearities, additional cross-correlation measurements were performed with the JNT system, which showed that the distortion tones could be modified by changing the dc signal provided to the input of the ADC. By increasing the dc offset of the signal from the original value of 85 mV to 125 mV, the even-order distortion increased about 10 dB. Although the distortion of the ADC was not systematically characterized, these results strongly suggest that the ADC dominates the non-linearity behaviour of the JNT electronics, at least for the specific even-order distortion tones that were observed when measuring the multi-tone odd-only comb waveforms.

4. Reducing non-linearities with QVNS waveforms

In section 3 it was shown how QVNS waveforms with low intrinsic distortion were used to reveal the specific sources of observable distortion so that electronics components with the dominant non-linearities could be removed. However, from the above measurements with the present electronics (configuration C), it is clear that non-linearities will always be present at some significant level and that the distortion is frequency dependent. These results imply that the distortion from non-linearities in the electronics will still dominate the measurement variance for comb waveforms with tone amplitudes of 35 nV. Thus, in order to further reduce the effects of non-linearities, another means is required other than replacing components and circuits with those having better linearity. One approach is to use synthesized pseudo-noise waveforms with higher density of tones that have closer tone spacing (smaller f_0). As the number of tones in a given bandwidth increases, their amplitudes decrease proportionally in order to keep the power spectral density constant. The resulting lower-amplitude tones will produce considerably smaller distortion from the same non-linearity. The effect of the distortion on the variance will fall as the density of QVNS-synthesized tones increases (1) because the amplitudes of the distortion products decrease (and more quickly for those of higher order) as the tone amplitudes decrease and (2) because the variance simply decreases for a larger number of tones. As was shown in figure 7(*a*), the second-order distortion should decrease twice as fast as the amplitude of the fundamental tones for two tones.

Figure 8 shows how the measurement standard deviations of the resistor-QVNS noise-power ratio depend on integration time for odd- and even-tone waveforms with different tone spacing ($2f_0$ = 3200 Hz, 800 Hz, 400 Hz and 200 Hz). The most important observation is that the measured standard deviations for waveforms with the smallest tone spacing more closely resemble the standard deviation expected for white noise for both odd- and even-tone waveforms. These QVNS-synthesized waveforms with higher tone density more closely reproduce the same non-linearities that are produced by the thermal noise. In addition, the inset shows that after an integration period of 80 000 s, the time-dependent measurement standard deviations for the even- and odd-tone waveforms decrease and closely approach the expected standard deviation for white noise as the tone spacing and amplitude decrease. In fact, the measurement standard deviation is nearly identical for odd- and even-tone waveforms, with the closest tone spacing ($2f_0$ = 200 Hz), indicating that the even-order distortion, in fact the total distortion, has been significantly reduced, and the measurement standard deviation follows the desired and expected behaviour of white noise.

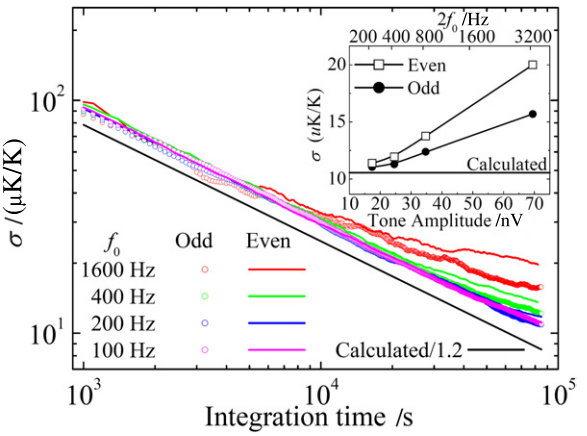

Figure 8. Measurement standard deviations of the resistor-QVNS noise-power ratio versus integration time for even-tone and odd-tone waveforms with different tone spacing ($2f_0$). The expected uncertainty (offset to calculated value/1.2) is also shown for comparison. The inset shows the resulting standard deviation after integrating for a period of 80 000 s as a function of the tone amplitude and $2f_0$ for both odd- and even-tone waveforms.

5. Summary

The improvements described in this paper have reduced some of the non-linearities of the measurement electronics, which resulted in lower measurement standard deviation for QVNS waveforms with higher tone density. It is important to note that the same absolute temperature for the water triple point was determined from measurements with each of these different waveforms (even-only, odd-only and with different tone spacing). The measured temperature was reproducible for the first time, indicating that we have at least reduced the effects of distortion to negligible levels. The measured temperature was always ∼50 μK/K higher than the ITS-90 temperature, which is larger than the previous result of 3 μK/K in 2007 with circuit configuration A. This larger temperature offset reveals an unresolved systematic error of the system, because the improvements of the present circuits (configuration C) have removed a possible aliasing error and reduced the effect of non-linearities. These results suggest that the 2007 result may have had a lower offset because of compensating systematic errors. Since the measured temperature is the same for different odd- and even-tone waveforms with different tone density, the present dominant systematic error does not appear to be caused by non-linearities in the measurement electronics. This

systematic error is probably produced by a yet undetected difference between the QVNS and sensing resistor input circuits, most likely in the transmission line between the QVNS and the preamplifiers.

In conclusion, the JNT cross-correlation electronics have been improved and the distortion from non-linearities in the cross-correlation electronics was successfully reduced by exploiting low-distortion QVNS-synthesized waveforms. Two-tone measurements showed that distortion still exists at some level in the measurement electronics, increasing the measurement variance, and that the second-order distortion is more significant than the other types of distortion. Odd-only multi-tone comb waveforms were shown to be useful for decreasing the effect of second-order distortion. However, the remaining non-linearities, predominantly from the ADC, still limited the measurement standard deviation. Finally, synthesized pseudo-noise waveforms with more closely spaced tones were shown to be effective at decreasing distortion from the non-linearities. By removing the stop-band alias systematic error, the reproducibility of the temperature measurements improved, but the measured value of the temperature of the water triple point moved further away from the expected ITS-90 value. Unfortunately, reducing the effect of non-linearities and improving the measurement variance for all pseudo-noise waveforms did not change this absolute temperature measurement, which suggests that the source of the remaining dominant systematic errors was not caused by non-linearities in the measurement electronics.

Acknowledgments

The authors thank Paul Dresselhaus, Charlie Burroughs, Weston Tew, Norm Bergren, Sae Woo Nam and Carl Williams for helpful discussions, collaboration and support.

Appendix. High-performance JFET amplifier

Because of the very low signal levels, the preamplifiers used for JNT have demanding requirements [13]. The power spectral density of the noise voltage of a 100 Ω resistor at the triple point of water (273.16 K) is about 1.23 nV $Hz^{-1/2}$, which is comparable to the input noise voltage of good low-noise JFET amplifiers. The use of cross-correlation eliminates the direct effect of the input noise voltage on the temperature measurement, but the noise still impacts measurement uncertainty and some systematic errors [13]. Primarily, the input stage of the amplifier must have a very low input noise current, which at high frequencies arises from the JFET channel noise and gate-channel capacitances. The input stage must operate without feedback to avoid undesirable correlations between the input noise voltage and input noise current. More typical preamplifier requirements are for a high input resistance to minimize the load on the resistor-noise source, and a high common-mode rejection ratio (CMRR) over the full measurement bandwidth to minimize the effects of any electromagnetic interference.

With increasing bandwidth and decreasing amplifier noise, the measurement time needed to achieve a certain statistical accuracy decreases. Thus, the preamplifier should have as little intrinsic noise and as large a bandwidth (e.g. at least 1 MHz) as is practical. The bandwidth of the measurement depends on the frequency dependence of both the amplifier and the input circuit, which is determined primarily by the sensor and QVNS resistances, the preamplifier input capacitance and the stray inductance and capacitance of the wiring. The amplifier must also be well shielded and be stable from oscillations over the whole observable frequency range, not just the measurement bandwidth.

The standard approach for JNT preamplifiers is to use low-noise JFETs in a differential common-source–common-base cascode arrangement and then to provide further amplification with instrumentation amplifiers realized with integrated operational amplifiers. The initial preamplifiers used by NIST [4–8], referred to as the '2006 amplifier' in [9, 11], were based on a JFET-cascode design developed by White and Zimmerman [13]. The design omitted the common-mode current source usually used in traditional differential amplifier stages, but achieved a very low noise current and low noise-voltage–noise-current correlation. However, because the design omits the common-mode current source, it has a relatively low CMRR, especially at the high frequencies employed in the NIST noise thermometer as the measurement bandwidth increased from 100 kHz towards 1 MHz. The new differential amplifier, shown in figure A1 and referred to as the '2007 amplifier' in [9, 11], includes the common-mode current source to greatly improve the CMRR, and eliminate the manual trimming of the CMRR. The current source also has the added benefit of improving the stability of the operating point for the JFETs. Like the original amplifier, the output signal of the input circuit is also amplified by an instrumentation-style amplifier. The whole circuit is battery-operated and protected by a simple control circuit.

The preamplifier input stage in figure A2 shows the differential JFET stage with bipolar-transistor cascode (at the top of the diagram) and the adjustable JFET common-mode current source (at the bottom of the diagram). Cascode amplifiers have a tendency to be unstable at high frequencies due to stray capacitances forming a Colpitt's oscillator. The combination of the use of surface mount components, a compact PCB layout, the low-impedance bias circuit for the cascode and the low common-mode gain all contribute to an improved stability. The input stage of the amplifier (see figure A2) was simulated for different load configurations, different input impedances and different bias modes with the SPICE-based LTspice simulator of Linear Technologies [19]. The entire preamplifier design, including the JFET input stage and the following instrumentation amplifier stage, was optimized for gain, wide bandwidth, high CMRR, low noise performance and stability. Series-connected LEDs were used to bias the cascode transistors. The simulated design was tested with the JFETs SNJ903L42 and was found to perform as expected (see table A1). The design was realized in the input stage of the amplifiers [20] used in the present noise thermometry setup. The measured noise floor of the amplifier is 0.85 nV $Hz^{-1/2}$, which is 23% lower than the 1.1 nV $Hz^{-1/2}$ noise floor of the 2006 amplifier. The new amplifier allows a

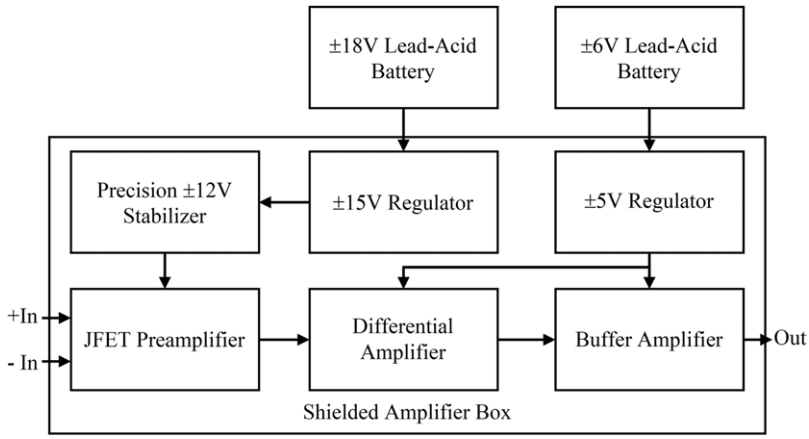

Figure A1. Block diagram of the new amplifier series.

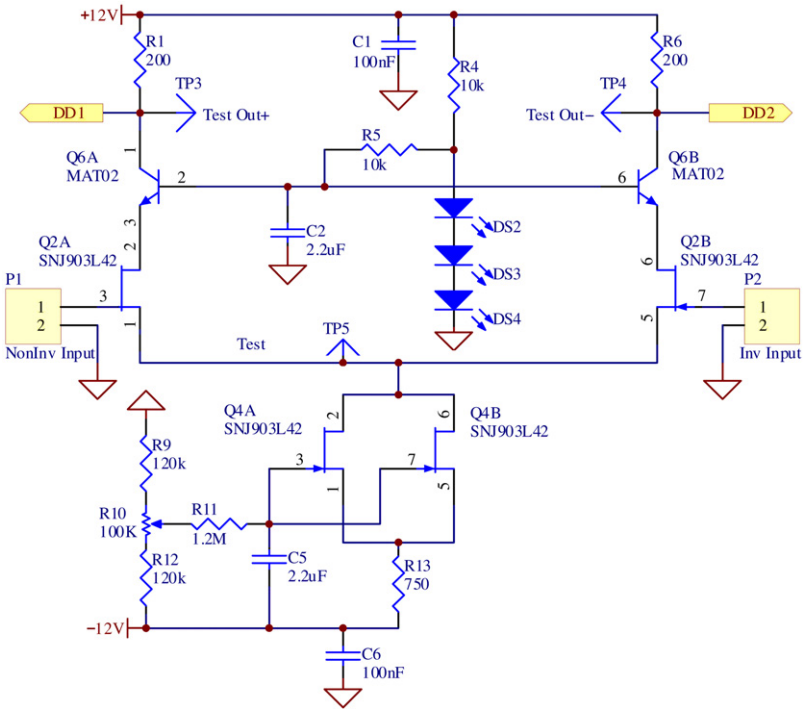

Figure A2. JFET differential input stage of the new differential amplifier. Q2A and Q2B as well as Q4A and Q4B are paired JFETS. Each pair is packed in a TO-78 metal can. P1 and P2 are the shielded differential inputs. DD1 and DD2 are outputs that connect to a differential op-amp stage.

Table A1. Simulated performance data of the JFET input stage and the buffer amplifier.

Amplifier	Frequency range −3 dB	Frequency range −1 dB	Voltage amplification into 50 Ω	Equivalent input noise (white noise regime)
Differential	10 Hz to 2 MHz	20 Hz to 1.2 MHz	70 dB	$<1\,\mathrm{nV\,Hz^{-1/2}}$
Buffer	10 Hz to 80 MHz	20 Hz to 10 MHz	0 dB	$4\,\mathrm{nV\,Hz^{-1/2}}$

higher 2.1 signal-to-noise (SNR) power ratio compared with the 1.2 SNR of the older 2006 amplifier. The resulting 2.4 dB decrease in the noise floor is useful for revealing distortion in the electronics and reduces the measurement time to 74% of that for the old amplifier, or equivalently a 13% lower measured variance for the same measurement time.

The main gain block is a classical wide-band instrumentation amplifier realized with the low-noise, low-distortion and moderate bandwidth operational amplifiers AD797 in a design optimized for bandwidth, symmetry and stability [21]. The bandwidth and amplification data are shown in table A1. Tests of the first generation of amplifiers showed that loading the output of the amplifier with a filter having 50 Ω impedance in series with the 50 Ω intrinsic output resistor of the amplifier seemed to lead to unacceptable distortion and instability at higher frequencies. A wide-band ac-coupled buffer amplifier

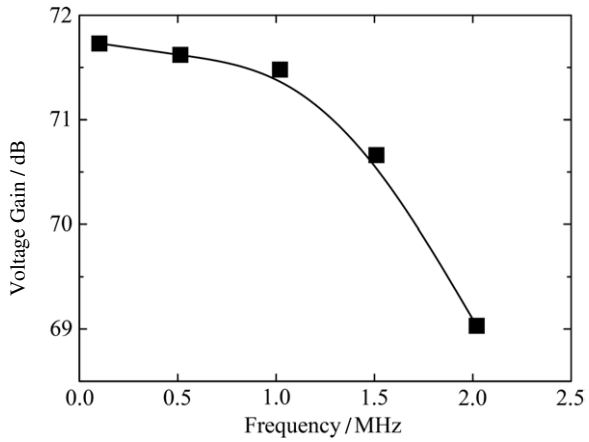

Figure A3. Typical gain as a function of frequency for the new differential amplifier.

was added to the output, which easily drives 50 Ω loads. In the new configuration, the observed distortion was drastically reduced and the system showed very stable operation.

The overall differential gain of the amplifier as a function of the frequency is shown in figure A3. The 1 dB point is reached at 1.2 MHz and the 3 dB point is at 2.0 MHz. The overall noise referred to the input is below 1 nV $Hz^{-1/2}$ in the white-noise regime. The CMRR is about 100 dB at 100 kHz. No instabilities could be observed in the frequency range up to 1 GHz. The usable output-voltage swing is limited to ±2 V, because at higher voltages the signal distortion becomes significant.

The power supply of the amplifier was designed for good decoupling of the different amplifier stages and for noise isolation of the input stage. The power sources are lead–acid batteries, which are located in a separate metal case about 1.5 m from the metal boxes containing the amplifiers. The nominal input voltages to the power supply for the input stage are ±18 V and ±6 V for the operational/buffer amplifier stages. The supply for the input stage is double stabilized. In the first stage, the nominal 18 V battery voltage is stabilized at 15 V with a peak-to-peak noise voltage of about 2 mV as measured on a 100 MHz-bandwidth oscilloscope. The second stabilizer is a precision stabilizer based on a design by Analog Devices [22]. In this version, it is used as a very low-noise ±12 V supply. Its noise voltage is 2 nV $Hz^{-1/2}$ measured at 100 kHz. Modern rail-to-rail operational amplifiers increase the stability range in this circuit for different load currents.

In addition to the new preamplifier, two buffer amplifiers that can drive 50 Ω reactive loads (amplifiers 1 and 2 in configuration C) are used to decouple the two 11-pole passive anti-alias filters before the ADC. The gains of these amplifiers were chosen to compensate attenuation from loading in the filter arrangement and to supply an additional gain of up to 20 dB, if desired. Integrated circuits AD811 [23] are used in the buffers, but even wider-bandwidth and lower-distortion circuit components have been demonstrated. The simulated performance data are shown in table A1. The buffers can be ac-coupled to prevent temperature-dependent offset voltages from propagating in the amplifier chain. Such an offset was observed in filter 2 (figure 1), which was found to change the operating point of the ADC. No contribution to the overall distortion could be measured from the high-quality ceramic coupling capacitors.

References

[1] Johnson J B 1927 Thermal agitation of electricity in conductors *Nature* **119** 50–1

[2] Nyquist H 1928 Thermal agitation of electric charge in conductors *Phys. Rev.* **32** 110–13

[3] White D R *et al* 1996 The status of Johnson noise thermometry *Metrologia* **33** 325–35

[4] Benz S P, Martinis J M, Nam S W, Tew W L and White D R 2002 A new approach to Johnson noise thermometry using a Josephson quantized voltage source for calibration *Proc. TEMPMEKO 2001* ed B Fellmuth *et al* (Berlin: VDE Verlag) pp 37–44

[5] Nam S W, Benz S P, Dresselhaus P D, Tew W L, White D R and Martinis J M 2003 Johnson noise thermometry measurements using a quantum voltage noise source for calibration *IEEE Trans. Instrum. Meas.* **52** 550–3

[6] Benz S P, Dresselhaus P D and Martinis J M 2003 An ac Josephson source for Johnson noise thermometry *IEEE Trans. Instrum. Meas.* **52** 545–9

[7] Nam S W, Benz S P, Dresselhaus P D, Burroughs C J, Tew W L, White D R and Martinis J M 2005 Progress on Johnson noise thermometry using a quantum voltage noise source for calibration *IEEE Trans. Instrum. Meas.* **54** 653–7

[8] Nam S W, Benz S P, Martinis J M, Dresselhaus P, Tew W L and White D R 2003 A ratiometric method for Johnson noise thermometry using a quantized voltage noise source *Temperature: its Measurement and Control in Science and Industry* vol 7 ed D C Ripple (New York: AIP) pp 37–44

[9] Benz S P, Qu J F, Rogalla H, White D R, Dresselhaus P D, Tew W L and Nam S W 2009 Improvements in the NIST Johnson noise thermometry system *IEEE Trans. Instrum. Meas.* **58** 884–90

[10] White D R and Benz S P 2008 Constraints on a synthetic-noise source for Johnson noise thermometry *Metrologia* **45** 93–101

[11] White D R, Benz S P, Labenski J R, Nam S W, Qu J F, Rogalla H and Tew W L 2008 Measurement time and statistics for a noise thermometer with a synthetic-noise reference *Metrologia* **45** 395–405

[12] Fischer J *et al* 2008 Preparative steps towards the new definition of the kelvin in terms of the Boltzmann constant *Int. J. Thermophys.* **28** 1753–65

[13] White D R and Zimmermann E 2000 Preamplifier limitations on the accuracy of Johnson noise thermometers *Metrologia* **37** 11–23

[14] White D R and Mason R S 2004 An EMI test for Johnson noise thermometry *Proc. TEMPMEKO 2004 (Zagreb)* ed D Zvizdic *et al* pp 485–90

[15] Toonen R C and Benz S P 2008 Characterizing the non-linear behaviour of single process components with precision multi-tones from a Josephson arbitrary waveform synthesizer, presented at the *Applied Superconductivity Conf. (Chicago, IL)*

[16] Benz S P, Burroughs C J and Dresselhaus P D 2000 Low harmonic distortion in a Josephson arbitrary waveform synthesizer *Appl. Phys. Lett.* **77** 1014–16

[17] Benz S P, Walls F L, Dresselhaus P D and Burroughs C J 2002 Low distortion waveform synthesis with Josephson junction arrays *IEICE Trans. Electron.* **85C** 608–10

[18] von Klitzing K, Dorda G and Pepper M 1980 New method for high-accuracy determination of the fine-structure

constant based on quantized Hall resistance *Phys. Rev. Lett.* **45** 494–7
[19] Ltspice IV is available from Linear Technologies, 1630 McCarthy Blvd, Milpitas, CA 95035-7417, USA (see http://www.linear.com/designtools/software/)
[20] The differential amplifiers, buffer amplifiers, and power supplies are from TSSE b.v., De Wilmskamp 2, 7552GC Hengelo, The Netherlands (see http://www.tsseshop.com)
[21] Datasheet AD797 (Rev. G, 09/2008) by Analog Devices: 3 Technology Way, Norwood, MA 02062, USA
[22] Jong W G 2005 *Op Amp Applications Handbook (Analog Devices Series)* (Oxford: Elsevier) ISBN 0-7506-7844-5
[23] Datasheet AD811 (Rev. E, 07/2004) by Analog Devices: 3 Technology Way, Norwood, MA 02062, USA